Journal of Materials Chemistry

Cite this: *J. Mater. Chem.*, 2012, **22**, 16416

www.rsc.org/materials

PAPER

Electrostatic interactions *versus* van der Waals interactions in the self-assembly of dispersed nanodiamonds†

Qian Xu and Xiang Zhao*

Received 9th May 2012, Accepted 19th June 2012
DOI: 10.1039/c2jm32918b

4–5 nm nanodiamonds tend to self-assemble into 100–200 nm nanodiamond aggregations and furthermore nanodiamonds in the early stages of the detonation process present fantastic twinned morphologies, indicating that there are strong interactions among these nanodiamonds. Herein, electrostatic interactions and van der Waals interactions between two nanodiamonds are explored using DFT computations in conjunction with Monte Carlo molecular simulations. It is indicated that the van der Waals forces are much stronger than the electrostatic forces for the unsaturated nanodiamonds. More importantly, two assembly features are exposed as follows: assembly has a preferential face-to-face orientation; assembly has a strong binding energy comparable to the dissociation energy of C–C bonding, which is -116.1 kcal mol^{-1} for a 2.48 nm truncated octahedral nanodiamond. The results suggest that the strong forces holding the nanodiamond aggregation almost certainly attribute to the proposed strong van der Waals forces, which is of great importance in understanding the aggregative properties of nanodiamond.

1. Introduction

Nanodiamonds were first produced in the 1960s in the U.S.S.R. from soot formed in explosions.[1] In such a production process, the explosion provides both the carbon source and conversion energy, leading to the advantages of being environment friendly, economic and suitable for mass production.[1,2] Since the late 1990s, nanodiamonds have become well-known to the world as having excellent mechanical properties for lubrication applications.[3] Recently, nanodiamonds have attracted enormous attention once again for their promising applications in industrial and biomedical fields such as chemical catalysis,[4] drug delivery[5,6] and biosensors.[7,8]

Nanodiamonds have diameters of 4–5 nm, but they tend to self-assemble into a nanodiamond aggregation of 100–200 nm. The size of nanodiamonds has been measured by dynamic light scattering (DLS) experiment, which presents a non-uniform distribution: a nanodiamond aggregation has the size of 100–200 nm, corresponding to the secondary particles of nanodiamond, in comparison with 4–5 nm of nanodiamond primary particles.[9,10] Furthermore, a nanodiamond aggregation can withstand strong ultrasonic treatment (2 kW).[9,11] In other words, ultrasonic treatment can separate a larger nanodiamond agglomeration into a 100–200 nm nanodiamond aggregation, but fails to purify a 100–200 nm nanodiamond aggregation into 4–5 nm primary nanodiamonds. Thus, the forces holding larger nanodiamond agglomerations must be van der Waals forces among the 100–200 nm nanodiamond aggregation, which can be destroyed by sonication. In turn, the forces holding the 100–200 nm nanodiamond aggregation among 4–5 nm primary nanodiamonds have been assumed to be chemical bonding, most likely C–C bonds.[9] Moreover, there is another fantastic self-assembly in the detonation process of nanodiamonds that small nanodiamond clusters tend to coalesce and thus form twinned nanodiamonds with preferential face-to-face interactions, and finally give rise to new grain boundaries.[11,12] The preferential interactions in such twinned nanodiamonds are frequently on the (111) planes.

In recent years, great progress on the purification methods of nanodiamond aggregation have been developed. By means of milling medium zirconia beads, Osawa, Krüger and co-workers successfully developed wet beads milling methods to disperse nanodiamond aggregations into 4–5 nm nanodiamonds.[10,13–15] Later, beads milling methods with a less expensive milling medium of sugar and salt achieved the dispersion too.[16] Besides, an alternative effective technique to purify nanodiamond was developed through selective surface oxidization to remove the non-diamond carbon and subsequently obtain the high purity 5 nm nanodiamond particles.[17] Ozone-purified nanodiamond is also reported to possess a low sp^2 content.[18] Moreover, centrifugation was used to accomplish the separation of nanodiamond agglomerates, as well as the formation of stable nanodiamond

Institute for Chemical Physics and Department of Chemistry, State Key Laboratory of Electrical Insulation and Power Equipment, Xi'an Jiaotong University, Xi'an 710049, China. E-mail: xzhao@mail.xjtu.edu.cn; Fax: +86-29-8266-8559; Tel: +86-29-8266-5671

† Electronic supplementary information (ESI) available: Comparison of universal force field and Dreiding force field calculation results. Comparison of DFT and SCC-DFTB method in calculating atomic charges of C_{548}. Comparisons of the relative contribution between electrostatic interaction and van der Waals interaction for larger nanodiamonds. See DOI: 10.1039/c2jm32918b

colloids.[19,20] Furthermore, surface reduction in a hydrogen atmosphere was attempted by Williams *et al.* to obtain 4 nm nanodiamond particles.[21] In addition to the hydrogenation reduction of nanodiamond, fluorination has also been performed in order to functionalize the nanodiamond surface and reduce the agglomeration of nanodiamond particles.[22–25] Among all of these methods, the beads milling methods rely on strong extra forces to break up nanodiamond aggregations, as well as selective surface oxidization, surface hydrogenation reduction and surface fluorination methods to modify the nanodiamond surface properties to decrease the tendency of reaggregation. In addition, the development of these purification methods in turn inspires the study of assembly features of nanodiamonds.

The underlying formation mechanism of nanodiamond aggregation has been heavily debated. It is usually believed that nanodiamond aggregation is the straightforward result of van der Waals type physical aggregates of nanodiamonds.[15,26–28] Nevertheless, some researchers suspected this point and considered that van der Waals forces should not be strong enough to bear ultrasonic treatment, and therefore attributed the nanodiamond aggregation to electrostatic interaction.[29,30] Barnard *et al.* presented a theoretical model with density functional tight binding-based calculations for the electrostatic potential of nanodiamond, and suggested that the electrostatic potential of bare nanodiamond depended on a surface index, leading to strong inter-particle electrostatic interactions and preferentially ordered self-assembled nanodiamond agglutination.[29,31–33] Thus, the electrostatic interactions contribute to the aggregation of primary nanodiamonds. However, lack of quantitative evaluation of van der Waals forces among nanodiamonds causes some difficulty in discerning the contributions between electrostatic interactions and van der Waals interactions. Besides, literature on silicon nitride particles suggests that in air electrostatic forces have been found to be insignificant compared to van der Waals interactions.[34,35] Hence, the effect of van der Waals cannot be simply ignored. Furthermore, to distinguish the contributions between electrostatic forces and van der Waals forces in the formation of nanodiamond aggregation becomes one of the fundamental and urgent questions in nanodiamond research.[11,36] Herein, we develop theoretical methods to make a quantitative estimation on both van der Waals interactions and electrostatic interactions to preliminarily discern their contributions in nanodiamond aggregation, as well as to explore the assembly features between nanodiamonds.

2. Computational methods

2.1. Molecular modelling of materials

At first, the structure of nanodiamonds was carefully examined. TEM results show that sphere and truncated octahedron are the two predominant morphologies in the nanodiamonds produced by detonation methods.[37] In these two morphologies, the truncated octahedral nanodiamond with bare surfaces has been determined to be more thermodynamically stable than spherical nanodiamonds if the size of nanodiamond molecule is larger than ~1.9 nm.[38] In this work, by cutting from perfect diamond crystal, three truncated octahedral nanodiamonds C_{548}, C_{837} and C_{1198} were built with diameters of 1.83 nm, 2.15 nm and 2.48 nm, respectively, as shown in Fig. 1 (d). Each of these structures contains six (100) faces and eight (111) faces. Moreover, due to structural asymmetry, the eight (111) faces can be divided into two types: the larger ones $(111)_L$ and the smaller ones $(111)_S$, as illustrated in Fig. 1(a)–(c). Furthermore, as truncated octahedral nanodiamond is a representative of polyhedral nanodiamond, the outcomes of the present study can be extended to the situation of other polyhedral nanodiamonds and even quasi-spherical nanodiamonds. Besides, it should be stressed that actually in only a few situations the surface of nanodiamond is probably clean, such as in the early stages of the detonation process as well as through thermal desorption of surface groups in inert gas in certain high temperature regions. In contrast, in most stages nanodiamonds are saturated by various groups. Even so, in the current work only clean nanodiamond models are selected, as firstly it is reported that clean, reconstructed nanodiamonds are thermodynamically more stable than hydrogenated nanodiamond between 2 and 3 nm;[39] secondly, such studies can expose the significant contribution to the self-assembly from the nanodiamond core rather than surface groups, and also corresponds to a few situations; and finally the study on the surface terminated nanodiamond models with distinct groups are still in progress, and preliminary results on hydrogenated nanodiamond and fluorinated nanodiamond do support the outcomes of the current work.

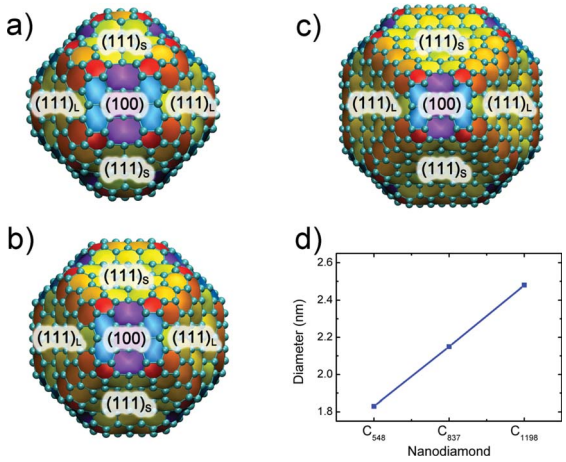

Fig. 1 Structure of relaxed nanodiamonds (a) C_{548}, (b) C_{837} and (c) C_{1198} as well as (d) their diameters.

All nanodiamond structures were fully relaxed before further calculations by density functional based tight binding with self-consistent charges (SCC-DFTB) method, with the convergence criterion of 10^{-8} a.u. $\approx$ 0.5 μeV A^{-1} for forces, implemented by dftb + code.[40,41] SCC-DFTB bases on the KS-DFTB scheme with a LCAO representation of the KS orbitals into the minimum basis set, where the orbitals are derived from a variational form of KS energy functional, a second-order Taylor expansion of density functional total energy with a pure exchange-correlation functional and respect to charge density fluctuations.[42] The zeroth order approach is equivalent to the non-self-consistent (TB) scheme. After the structural relaxation, carbon atoms on the (100) surfaces went through 2 × 1 reconstructions, as presented in Fig. 1(a)–(c) rendered by the VMD package.[43] Meanwhile, the (111) surfaces went on to graphitization, as indicated in our previous study.[44]

2.2. Molecular simulation and Mulliken charge calculation

Since precisely calculating non-bond interactions by first-principle methods is very computationally expensive, an approximation scheme *via* a force field based method to estimate the non-bond interaction energy between nanodiamonds is employed, where van der Waals interactions and electrostatic interactions are described by the Lennard–Jones potential and atomic monopoles with a distance-dependent Coulomb term, respectively. Besides, atomic Mulliken charges of nanodiamond C_{548} are computed by *ab initio* density functional theory calculations at the B3LYP/STO-3G level of theory[45–47] in the Gaussian 03 program package.[48]

In this work, molecular simulations were carried out using Blends module of Materials Studio. Universal force field was used to calculate interatomic interactions with the charges assigned from calculated atomic Mulliken charges. A large number of configurations (10^7 samples) of the two nanodiamond particles were generated and each of the corresponding binding interactions was calculated to search out the lower energy configurations. Furthermore, in order to verify the independence of simulation results on the different force fields, the Dreiding force field was employed too, as discussed in the ESI†.

3. Results and discussion

3.1. Assembly modes between nanodiamonds

The preferential assembly configurations between two nanodiamond C_{548} particles were explored by the Monte Carlo method. In the 100 lower energy configurations of all possible 10^7 samples, we find that only two assembly modes exist: $(111)_L$–$(111)_S$ and $(111)_S$–$(111)_S$, with a proportion of 3 : 7, as illustrated in Fig. 2(a), which agree well with previous experimental observations and theoretical reports.[29,33] In addition, these two modes both exhibit a (111)–(111) face-to-face configuration, which is conjectured to be the results of maximum surface contact. Therefore, it is expected that maximum surface contact can be treated as a rule to distinguish the favoured energy configurations.

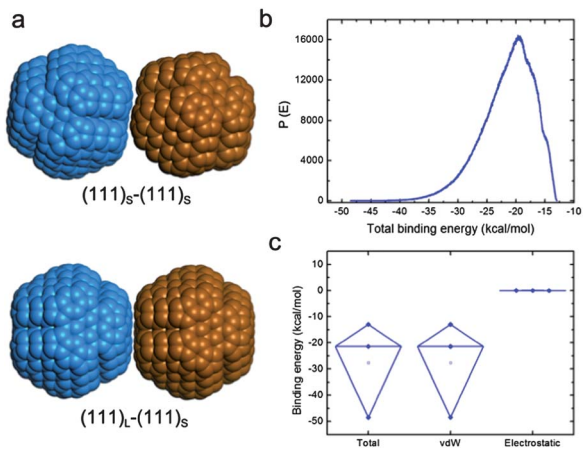

Fig. 2 (a) Assembly modes of two nanodiamond C_{548} particles; (b) total binding energy distribution and (c) ranges of total, van der Waals and electrostatic interaction energies of nanodiamond C_{548}, the horizontal lines indicate the average binding energies, and the range of electrostatic interaction energies is so small that the upper limit and lower limit almost overlap.

On the other hand, there are a total of three possible surface contact modes between the two types of (111) surface: $(111)_L$–$(111)_L$, $(111)_L$–$(111)_S$ and $(111)_S$–$(111)_S$. But the $(111)_L$–$(111)_L$ configuration was not found in the 100 low energy configurations, suggesting that the $(111)_L$–$(111)_L$ assembly mode does not possesses any energy advantages and the maximum surface contact rule is necessary but is insufficient in determining the favoured energy configurations. Even so, these results indicate a general assembly feature of nanodiamonds that the particles have preferred specific orientations related to one another. In this sense, the assembly between nanodiamonds exhibits a feature of directionality.

Furthermore, this feature can be extended to other polyhedral nanodiamonds that the energy preferential assembly modes for polyhedral nanodiamonds possess face-to-face configurations. Finally, as a result of the directional feature and steric hindrance effect, nanodiamonds have limited coordination numbers, which is indicated to be 5.521 ± 0.008 for nanodiamond C_{548} by results of coordination number calculations, as shown in Fig. 4(c).

3.2. Binding energy

The directional feature of nanodiamond self-assembly can be further analyzed from the distribution of binding interaction energies, as shown in Fig. 2(b). Firstly, the binding energies of nanodiamond C_{548} range from -48.5 to -12.9 kcal mol^{-1}, suggesting the most stable non-bond interaction is as strong as chemical bonds. As indicated from the maximum surface contact rule, such a strong non-bond attraction (-48.5 kcal mol^{-1}) comes from the relatively large surface areas of nanodiamond. Secondly, the effect of the relative position of two nanodiamond particles on the binding energies can be demonstrated from the binding energy distribution, as simulation samples are generated within the constraint that two particles contact each other on the van der Waals surface. In detail, the energetically preferred configurations, with the preferential assembly modes of face-to-face interaction, have very stable binding energies as large as -48.5 kcal mol^{-1}. On the contrary, binding energies of the energetically inferior configurations are as small as -12.9 kcal mol^{-1}. Such an energy difference is attributed to relative positions. Notably, the weak binding energy (-12.9 kcal mol^{-1}) is remarkably larger than common non-bond interactions in small molecules. Hence, these results emphasize that the directional feature is driven by the principle of minimum total potential energy. As a brief summary, two important assembly features between nanodiamond particles are exhibited that the assembly is directional and the assembly has a much larger binding interaction energy.

3.3. Van der Waals interactions *versus* electrostatic interactions

In this work, the binding interactions between nanodiamond particles belong to non-bond interactions which consist of van der Waals interactions and electrostatic (Coulombic) interactions. Van der Waals force is the sum of the attractive and the

repulsive non-bond forces between atoms or molecules other than the electrostatic forces. Although the van der Waals force between two carbon atoms is very weak, there are a lot of van der Waals forces between two particles, leading to a very strong interaction.

The contributions from the van der Waals interactions and electrostatic interactions to the total binding interaction energy are illustrated in Fig. 2(c). It is clear that the total interaction and the van der Waals interaction almost share the same range of binding energy within from −48.5 to −12.9 kcal mol^{-1}. In contrast, the electrostatic interaction is very weak with a range from −0.01 to 0.02 kcal mol^{-1}, suggesting that in some samples the electrostatic force appears as an attractive force and in the other samples exhibits as a repulsive force. It should be noticed that the atomic Mulliken charges from *ab initio* density functional theory calculations depend on the specific density-functional and basis sets. Nevertheless, the tendency and relative value of the atomic Mulliken charges among different density-functional and basis sets stay similar. Considering that the contributions from van der Waals interaction are much larger than the one from electrostatic interaction, it is reasonable to conclude that the non-bond interaction between two nanodiamond particles is driven by van der Waals forces rather than electrostatic forces.

In order to evaluate the attractive and repulsive electrostatic interactions, atomic Mulliken charge distribution and electrostatic potential of bare nanodiamond C_{548} are further investigated, as illustrated in Fig. 3(a) and (b). According to different surface index and symmetry, the Mulliken charge distribution and electrostatic potential can be classified into three types: (100) type, $(111)_L$ type and $(111)_S$ type. Furthermore, as the same type faces have the same electrostatic features, these special face to face contacts including (100)–(100), $(111)_L$–$(111)_L$ and $(111)_S$–$(111)_S$ lead to an electrostatic repulsive interaction. For the case of nanodiamond C_{548}, the two most stable binding interaction modes are $(111)_L$–$(111)_S$ and $(111)_S$–$(111)_S$. The latter one possesses an electrostatic repulsive interaction. However, whether the electrostatic interaction of the former one is attractive or repulsive depends on the specific electrostatic features. The blends calculation results confirm this theory as shown in Fig. 3(c) that the $(111)_L$–$(111)_S$ face to face interaction possesses an electrostatic attractive interaction of −0.008 kcal mol^{-1}, but the $(111)_S$–$(111)_S$ face to face interaction has an electrostatic repulsive interaction of 0.0002 kcal mol^{-1}, as illustrated in Fig. 3(d). It should be noted that the ranges of surface electrostatic potentials and atomic Mulliken charges calculated by *ab initio* density functional theory in our work is much smaller than that calculated by semi-empirical SCC-DFTB methods in literature,[29,31] which is believed to be caused by the SCC-DFTB methods which overestimate these values. Consequently, the SCC-DFTB methods overestimate the electrostatic interactions between nanodiamonds.[29,30] The difference between DFT and SCC-DFTB methods in calculating atomic charges of C_{548} is discussed in the ESI†.

3.4. Assembly features for larger nanodiamonds

The assembly features of larger nanodiamond particles of C_{837} and C_{1198} are also examined and the results are illustrated in Fig. 4. Considering that the total binding energy is almost equal to the van der Waals binding energy, the contributions from electrostatic interaction are therefore ignored in the binding energy calculations for these larger nanodiamonds. In addition, quantitative comparisons on the relative contributions of electrostatic interaction and van der Waals interaction for larger nanodiamonds are supplied in the ESI†.

Firstly, our results exhibit that nanodiamond C_{837} and C_{1198} possess strong non-bond interactions similar to the situation of nanodiamond C_{548}. As shown in Fig. 4(a), C_{548}, C_{837} and C_{1198} take maximum binding energies of −48.5, −85.8 and −116.1 kcal mol^{-1}, respectively. The binding energy of −116.1 kcal mol^{-1} is even larger than the bond-dissociation energy of a C–C bond, which is 83–85 kcal mol^{-1}. This result suggests that the non-bond interactions between nanodiamond particles can be even stronger than chemical bonds, because it comes from the accumulation of a lot of van der Waals interactions.

Secondly, the bigger the nanodiamond particles are, the larger the corresponding binding energies are. In detail, as indicated in

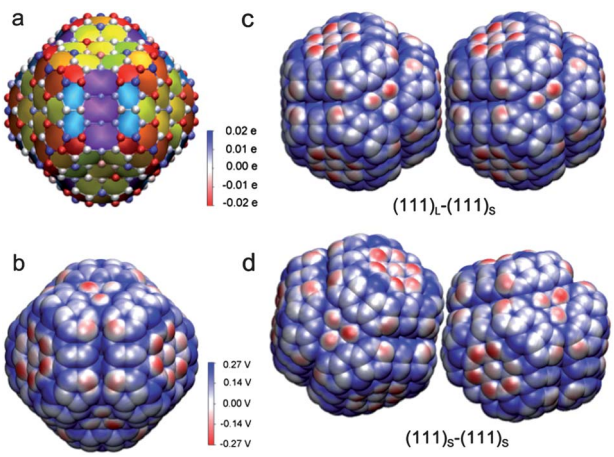

Fig. 3 (a) Mulliken charge distribution, (b) electrostatic potential, (c) electrostatic interaction of $(111)_L$–$(111)_S$ assembly mode and (d) $(111)_S$–$(111)_S$ assembly mode of nanodiamond C_{548}.

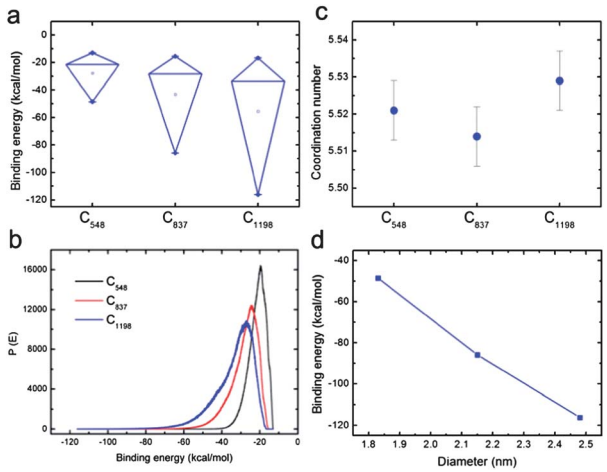

Fig. 4 (a) and (b) Binding energy distribution and (c) coordination number of nanodiamond C_{548}, C_{837} and C_{1198} as well as (d) effect of nanodiamond size on the binding energy.

Fig. 4(a), (b) and (d), the average binding energies, the most probable binding energies, and the most stable binding energies all increase when the particles size increases from 1.83 nm for C_{548} to 2.48 nm for C_{1198}. In particular, the most stable binding energies grow very fast, as presented in Fig. 4(d). Hence, it is feasible to predict that the 4–5 nm primary nanodiamonds also possess a strong binding energy.

Thirdly, the binding energies of quasi-spherical nanodiamonds can be roughly evaluated from the average energy and the most probable binding energies of truncated octahedral nanodiamond. As presented in Fig. 4(b), the average binding energies and the most probable binding energies increase slowly and always drop into the energy range of from −20 to −40 kcal mol^{-1} as the sizes of nanodiamond particles grow up from 1.83 nm to 2.48 nm. As a result, the binding energy in the nanodiamond aggregation highly depends on the specific morphologies and the quasi-spherical nanodiamonds possess a binding energy of about from −20 to −40 kcal mol^{-1}.

Fourthly, the structure of a nanodiamond aggregation is much more complicated than the structure of covalent crystals. Truncated octahedral nanodiamond particles of C_{548}, C_{837} and C_{1198} are indicated to possess a coordinate number of 5.5, as shown in Fig. 4(c). Furthermore, combining the directional property and steric hindrance effect, nanodiamonds are unlikely to form the nanodiamond aggregation entirely by ideal assembly modes. Thus, further progress is still needed on the distribution of ideal assembly modes in nanodiamond aggregation.

4. Conclusions

As a conclusion, we reveal that the assembly interactions between nanodiamond particles are dominated by van der Waals forces rather than electrostatic forces. Furthermore, two assembly features between polyhedral nanodiamond particles are exposed that the assembly mode is directional with preferential face-to-face interaction, and the assembly has strong binding energies comparable to the dissociation energy of C–C chemical bonds. Moreover, as the size of the nanodiamond particles become bigger, the most stable binding energies grow very fast, while the average binding energies and most probable binding energies increase very slowly, leading to a non-uniform binding energy distribution and complex structure in nanodiamond aggregation.

These outcomes shed light on the understanding of some experimental phenomena of nanodiamonds. As addressed above, there are strong forces holding nanodiamonds in a nanodiamond aggregation, which can even withstand a strong ultrasonic treatment. In this work, we found that the non-bond interactions between nanodiamond particles possess two important assembly features of directionality and strong binding energy, agreeing very well with the characters of the strong forces. In particular, the binding energies in the ideal assembly modes are remarkably large and probably possess the ability to withstand such an ultrasonic effect. Thus, the strong forces are almost certainly attributed to the strong binding forces. In addition, the fantastic self-assembly in the detonation process which leads to the formation of twinned nanodiamonds with preferential (111)/(111) interactions can also be mainly explained by the proposed strong non-bond interactions. Moreover, numerous experimental reports present that oxidization, hydrogenation and fluorination of nanodiamond aggregation can accelerate the dispersion process. Nevertheless, the mechanisms of these approaches have not been exposed. Based on this work, it is known that van der Waals forces make a great contribution to the assembly. Consequently, approaches on decreasing the van der Waals forces can facilitate the purification process. The approaches of oxidization, hydrogenation and fluorination modify the surface structure and properties, as well as break the maximum surface contact rule, which could remarkably decrease van der Waals forces and easily perform the dispersion process.

Acknowledgements

This work was financially supported by National Natural Science Foundation of China (21171138), the National Key Basic Research Program of China (2012CB720904) and the Key Project in the National Science and Technology Pillar Program of China (2010BAK67B12).

Notes and references

1 V. Danilenko, *Phys. Solid State*, 2004, **46**, 595–599.
2 A. Krueger, *Adv. Mater.*, 2008, **20**, 2445–2449.
3 N. R. Greiner, D. S. Phillips, J. D. Johnson and F. Volk, *Nature*, 1988, **333**, 440–442.
4 J. Zhang, D. S. Su, R. Blume, R. Schlögl, R. Wang, X. Yang and A. Gajović, *Angew. Chem., Int. Ed.*, 2010, **49**, 8640–8644.
5 H. Huang, E. Pierstorff, E. Osawa and D. Ho, *Nano Lett.*, 2007, **7**, 3305–3314.
6 X. Q. Zhang, R. Lam, X. Xu, E. K. Chow, H.-J. Kim and D. Ho, *Adv. Mater.*, 2011, **23**, 4770–4775.
7 J. R. Maze, P. L. Stanwix, J. S. Hodges, S. Hong, J. M. Taylor, P. Cappellaro, L. Jiang, M. V. G. Dutt, E. Togan, A. S. Zibrov, A. Yacoby, R. L. Walsworth and M. D. Lukin, *Nature*, 2008, **455**, 644–647.
8 W. Yang, O. Auciello, J. E. Butler, W. Cai, J. A. Carlisle, J. E. Gerbi, D. M. Gruen, T. Knickerbocker, T. L. Lasseter, J. N. Russell, L. M. Smith and R. J. Hamers, *Nat. Mater.*, 2002, **1**, 253–257.
9 E. Ōsawa, *Pure Appl. Chem.*, 2008, **80**, 1365–1379.
10 M. Ozawa, M. Inaguma, M. Takahashi, F. Kataoka, A. Krüger and E. Ōsawa, *Adv. Mater.*, 2007, **19**, 1201–1206.
11 V. N. Mochalin, O. Shenderova, D. Ho and Y. Gogotsi, *Nat. Nanotechnol.*, 2012, **7**, 11–23.
12 O. A. Shenderova and D. M. Gruen, *Ultrananocrystalline Diamond–Synthesis, Properties, and Applications*, William Andrew Publishing, 2006.
13 A. Krueger, *J. Mater. Chem.*, 2008, **18**, 1485–1492.
14 Y. Liang, M. Ozawa and A. Krueger, *ACS Nano*, 2009, **3**, 2288–2296.
15 A. Krüger, F. Kataoka, M. Ozawa, T. Fujino, Y. Suzuki, A. E. Aleksenskii, A. Y. Vul and E. Osawa, *Carbon*, 2005, **43**, 1722–1730.
16 A. Pentecost, S. Gour, V. Mochalin, I. Knoke and Y. Gogotsi, *ACS Appl. Mater. Interfaces*, 2010, **2**, 3289–3294.
17 S. Osswald, G. Yushin, V. Mochalin, S. O. Kucheyev and Y. Gogotsi, *J. Am. Chem. Soc.*, 2006, **128**, 11635–11642.
18 O. Shenderova, A. Koscheev, N. Zaripov, I. Petrov, Y. Skryabin, P. Detkov, S. Turner and G. Van Tendeloo, *J. Phys. Chem. C*, 2011, **115**, 9827–9837.
19 A. E. Aleksenskiy, E. D. Eydelman and A. Y. Vul, *Nanosci. Nanotechnol. Lett.*, 2011, **3**, 68–74.
20 Y. Morita, T. Takimoto, H. Yamanaka, K. Kumekawa, S. Morino, S. Aonuma, T. Kimura and N. Komatsu, *Small*, 2008, **4**, 2154–2157.
21 O. A. Williams, J. Hees, C. Dieker, W. Jager, L. Kirste and C. E. Nebel, *ACS Nano*, 2010, **4**, 4824–4830.
22 Y. Liu, Z. Gu, J. L. Margrave and V. N. Khabashesku, *Chem. Mater.*, 2004, **16**, 3924–3930.
23 Y. Liu, V. N. Khabashesku and N. J. Halas, *J. Am. Chem. Soc.*, 2005, **127**, 3712–3713.

24 M. A. Ray, O. Shenderova, W. Hook, A. Martin, V. Grishko, T. Tyler, G. B. Cunningham and G. McGuire, *Diamond Relat. Mater.*, 2006, **15**, 1809–1812.
25 H. Huang, Y. H. Wang, J. B. Zang and L. Y. Bian, *Appl. Surf. Sci.*, 2012, **258**, 4079–4084.
26 H. Huang, L. Dai, D. H. Wang, L.-S. Tan and E. Osawa, *J. Mater. Chem.*, 2008, **18**, 1347–1352.
27 O. A. Shenderova and S. A. Ciftan Hens, in *Nanodiamonds: Applications in Biology and Nanoscale Medicine*, ed. D. Ho, Springer, New York, 2010, pp. 79–116.
28 H.-D. Wang, Q. Yang and C. H. Niu, *Diamond Relat. Mater.*, 2012, **25**, 73–79.
29 A. S. Barnard, *J. Mater. Chem.*, 2008, **18**, 4038–4041.
30 L. Lai and A. S. Barnard, *J. Phys. Chem. Lett.*, 2012, **3**, 896–901.
31 A. S. Barnard and M. Sternberg, *J. Mater. Chem.*, 2007, **17**, 4811–4819.
32 E. Osawa, D. Ho, H. Huang, M. V. Korobov and N. N. Rozhkova, *Diamond Relat. Mater.*, 2009, **18**, 904–909.
33 L. Y. Chang, E. Osawa and A. S. Barnard, *Nanoscale*, 2011, **3**, 958–962.
34 G. Kumar, S. Smith, R. Jaiswal and S. Beaudoin, *J. Adhes. Sci. Technol.*, 2008, **22**, 407–428.
35 R. P. Jaiswal, G. Kumar, C. M. Kilroy and S. P. Beaudoin, *Langmuir*, 2009, **25**, 10612–10623.
36 V. Bondar' and A. Puzyr', *Phys. Solid State*, 2004, **46**, 716–719.
37 V. L. Kuznetsov, A. L. Chuvilin, E. M. Moroz, V. N. Kolomiichuk, S. K. Shaikhutdinov, Y. V. Butenko and I. Y. Mal'kov, *Carbon*, 1994, **32**, 873–882.
38 A. S. Barnard and P. Zapol, *J. Chem. Phys.*, 2004, **121**, 4276–4283.
39 J. Y. Raty and G. Galli, *Nat. Mater.*, 2003, **2**, 792–795.
40 B. Aradi, B. Hourahine and T. Frauenheim, *J. Phys. Chem. A*, 2007, **111**, 5678–5684.
41 M. Elstner, D. Porezag, G. Jungnickel, J. Elsner, M. Haugk, T. Frauenheim, S. Suhai and G. Seifert, *Phys. Rev. B: Condens. Matter*, 1998, **58**, 7260.
42 G. Seifert, *J. Phys. Chem. A*, 2007, **111**, 5609–5613.
43 W. Humphrey, A. Dalke and K. Schulten, *J. Mol. Graphics*, 1996, **14**, 33–38.
44 L. S. Li and X. Zhao, *J. Chem. Phys.*, 2011, **134**, 044711.
45 A. D. Becke, *Phys. Rev. A: At., Mol., Opt. Phys.*, 1988, **38**, 3098–3100.
46 A. D. Becke, *J. Chem. Phys.*, 1993, **98**, 5648–5652.
47 C. Lee, W. Yang and R. G. Parr, *Phys. Rev. B*, 1988, **37**, 785–789.
48 J. Frisch, G. W. Trucks, H. B. Schlegel, G. E. Scuseria, M. A. Robb, J. R. Cheeseman, J. A. Montgomery, T. Vreven, K. N. Kudin, J. C. Burant, J. M. Millam, S. S. Iyengar, J. Tomasi, V. Barone, B. Mennucci, M. Cossi, G. Scalmani, N. Rega, G. A. Petersson, H. Nakatsuji, M. Hada, M. Ehara, K. Toyota, R. Fukuda, J. Hasegawa, M. Ishida, T. Nakajima, Y. Honda, O. Kitao, H. Nakai, M. Klene, X. Li, J. E. Knox, H. P. Hratchian, J. B. Cross, V. Bakken, C. Adamo, J. Jaramillo, R. Gomperts, R. E. Stratmann, O. Yazyev, A. J. Austin, R. Cammi, C. Pomelli, J. W. Ochterski, P. Y. Ayala, K. Morokuma, G. A. Voth, P. Salvador, J. J. Dannenberg, V. G. Zakrzewski, S. Dapprich, A. D. Daniels, M. C. Strain, O. Farkas, D. K. Malick, A. D. Rabuck, K. Raghavachari, J. B. Foresman, J. V. Ortiz, Q. Cui, A. G. Baboul, S. Clifford, J. Cioslowski, B. B. Stefanov, G. Liu, A. Liashenko, P. Piskorz, I. Komaromi, R. L. Martin, D. J. Fox, T. Keith, A. Laham, C. Y. Peng, A. Nanayakkara, M. Challacombe, P. M. W. Gill, B. Johnson, W. Chen, M. W. Wong, C. Gonzalez and J. A. Pople, *Gaussian 03 (Revision E.01)*, Gaussian, Inc., Wallingford CT, 2004.